NUMERICAL AND EXPERIMENTAL INVESTIGATIONS OF FORMING LIMIT DIAGRAMS IN METAL SHEETS

بحث عددي وتجريبي لمنحنيات حد التشكيل لألواح معدنية

M. Samuel

Dept. of Production Engineering and Machine Design, Faculty of Engineering, Mansoura University. Post Code 35516, Mansoura, Egypt, Fax No. +2050 224 46 90&E-Mail: magdy_samuel@hotmail.com

ملخص البحث: يعتبر حد انفعال التشكيل هو المعيار الواسع الاستخدام في الصناعة لقياس استقرارية المعدن المُشكل بالأخذ في الاعتبار نمو تمركز التعنق قبل انهيار المعدن. هذا المعيار مناسب تماما للاستخدام في عمليات التشكيل التي يكون فيها مسار الانفعال خطي ، ولكن في عمليات التشكيل الامتطاطية لن يكون مسار الانفعال خطيا أبدا. لهذا فان استخدام هذا المعيار لكل عمليات التشكيل دون النظر لعلاقة مسارات الانفعال بها يسبب تقييم خاطئ يؤدى إلى خطورة شديدة لعملية التشكيل. في هذا البحث تم دراسة عدديه باستخدام تحليل العناصر المحددة الصريحة explicit والضمنية implicit مع برنامج مارك MARC ثلاثي الأبعاد لنموذج أُعدّ للتنبوء بكل من منحيات حد الانفعال والإجهاد وكذلك توزيع السمك عند تشكيل عميق باستخدام سمبك مُربع وأخر أسطواني لمعدني الصلب والألومنيوم السبائكي. أظهرت النتائج تطابق تام بين كل من الدراسة النظرية والعملية ويمكن تفسير ذلك بدقة النموذج المُستخدم وقدرته علي التنبوء وسرعة استجابته للمتغيرات المُختلفة أثناء عملية التشكيل.

ABSTRACT

A strain forming limit criterion is widely used throughout the sheet metal forming industry to gauge the stability of the deformed material with respect to the development of a localized neck prior to fracture. This criterion is strictly valid only when the strain path is linear throughout the deformation process. There is significant data that shows a strong and complex dependence of the limit criterion on the strain path. But unfortunately, the strain path is never linear in secondary forming processes. Furthermore, the path is often to be nonlinear in localized critieal areas in the first draw die. Therefore, the conventional practice of using a path independent strain forming diagram criterion often leads to erroneous assessments of severity forming process. In this study, the numerical results are based on MARC K7.1-3D finite element analysis (FEA) software using rigid-plastic flow method. This general purpose of FEA code is using both the implicit and explicit procedure. The model is employed to predict the stress- strain forming limit diagrams and thickness distribution of a deep drawing quality steel (DDQS) and aluminium alloy (AL) sheets. The predicted results agree well with those determined experimentally.

Keywords: Forming limit, Numerical simulation, MARC K7.1-3D FEA, Implicit and explicit procedure.

1. INTRODUCTION

Sheet metal forming process is an important technology in manufacturing, especially in the automotive industry. A number of parameters affect the formability of sheet metal. Most of metal sheet forming processes may be charactrised by nonlinear problem in geometry, material behavior, and extensive sliding friction contact phenomena. Knowledge of the deformation mechanism and the influence of the process parameters are important in the design of sheet metal forming processes. Numerical simulation of sheet metal forming processes is generally carried out by the finite element method (FEM). Since sheet metal undergoes large plastic strain deformation and rotation with stretching and bending into a very complicated shape during the forming process, thus the FEA is inevitably necessary for the more precise sheet forming analysis. From point of view, the formability of sheet metal is critical to a successful sheet forming operation, for which the forming limit diagram (FLD) is well known and is widely applied. The FLD defines, in a way, the onset of localized necking, which may be used as a measure of the maximum formability of sheet metal. Since 1970's, finite element theories have been developed for providing the useful information to the real processes in industries [1-11]. The FEA usually gives the information of forming process such as the deformed

Accepted May 19, 2003.

shape, strain and stress distribution, punching load, and the fracture. But, it is very difficult to determine the process parameters before the manufacturing because forming processes are effected by the process parameters such as the forming tool geometry, the blank shape, the blank holding force, and sliding friction between blank and forming tools. Despite the importance of the process parameter deformation, information yet relies on the experience and the intuition or the time consuming computer analysis such as incremental FE methods for small modification after the process design. Generally, it is very difficult to determine the optimum parameters for satisfying the design specification without any problem during the forming process. Recently, many researches have been carried out with the FEA and the optimization techniques [12-24].

In this study, the forming analysis was performed with MARC K7.1 FEA package using rigid-plastic flow method. A rigid-plastic FE formulation with planar anisotropy obeying equivalent Von Mises yield criterion with the plane stress assumption is adopted [25]. Also, the bending energy term with planar anisotropy is used [26].

The aim of the paper is to show that the computational approach developed during this study can be used successfully to simulate the deep drawing process for a different range of materials used in real forming applications. Validation of the comprehensive numerical simulations was performed by comparison with experimental results for important process parameters, namely strain and stress forming diagrams, blank shape, and thickness distribution.

2. EXPERIMENTS

2.1 Metals

Two sheet metals were chosen for the experimental deep drawing; a deep drawing quality steel (DDQS) and an aluminium alloy (AL). The mechanical properties of the test materials are tabulated in Table 1.

The plastic anisotropy of the materials was described by the R-value for 0^0,45^0, and 90^0 to the rolling direction.

$$R = (R_0 + 2R_{45} + R_{90})/4 \tag{1}$$

In order to describe the strain hardening and strain rate hardening behaviour of metals, the equivalent strain rate, $\dot{\bar{\varepsilon}}$, is expressed in terms of the equivalent stress, $\bar{\sigma}$, or

$$\dot{\bar{\varepsilon}} = \dot{\varepsilon}_0 \left[\bar{\sigma}/K\right]^{1/m} \tag{2}$$

where m is known as the strain rate sensitivity of flow stress; the effective flow stress, K, and the reference strain rate, $\dot{\varepsilon}_0$, are defined below. The effective flow stress, K, and its dependence on equivalent plastic strain, $\bar{\varepsilon}$, can be determined from a uniaxial tension test at a reference strain rate, $\dot{\varepsilon}_0$. If has been demonstrated that a number of experimental data could be represented most accurately by the well-known Swift equation [27] or

$$K = K_0(\varepsilon_0 + \bar{\varepsilon})^n \tag{3}$$

where K_o and ε_o are material constants and n is the strain hardening exponent. Equations (2) and (3) can now be combined to express the equivalent stress, $\bar{\sigma}$, in terms of variations in $\dot{\bar{\varepsilon}}$ and $\bar{\varepsilon}$. This model gives a good description for the deep drawing quality steel (DDQS) [28], while for the aluminium, more advanced models are sometimes advocated. Equations 2 and 3 were, however, used for metals in this investigation.

2.2 Deep Drawing Experimental Tests

Deep drawings of cylindrical flat and square punches were performed with tool geometry shown in Fig.1. The dimensions of each circular and square blank are 100-mm diameter and 100x100-mm lengths with round corner respectively. Each blank was lubricated on both sides and pressed at a 25 $mm.s^{-1}$. For lubricant, a high viscous drawing oil was used. A 4 mm square grid pattern included contact circles, each of 2 mm in diameter, was etched photo-chemically on the blanks before deformation to facilitate measurement of the strain distribution on the surface of the blank after forming.

The experiments were conducted on an electro-hydraulic servo controlled ± 100 KN-MTS at room temperature. Experimental results are used to verify the FEM.

3 EVALUATION MODELS

3.1 Forming Limit Evaluation

The reduction of spoilage during sheet metal forming operations needs modern methods of processes design. Significant progress in the field of design can be achieved by the development of a better method of calculation of sheet metal formability and method of precis determination of strain and stress distributions in deformed parts.

Table 1. Mechanical properties of the sheet metals

Material	Yield stress (MPa)	UTS (MPa)	Elongation (%)	n	K (MPa)	R	E (GPa)	Thick. (mm)	ν	ε_o
DDQS	220	330	40	0.18	547	1.65	210	0.85	0.30	0.00712
AL	177	200	25	0.22	388	0.87	70.1	0.85	0.33	0.01660

There are several criteria that can be used to compute the forming limits, such as the plastic instability, the classical bifurcation analysis, and that necking develops from loeal regions of initial nonuniformity. Hill [29] analysed bifurcation corresponding to localized necking using classical (smooth yield surface and normality) rigid-plasticity theory. According to this theory, localized will not occur in a sheet metal subjected to positive biaxial stretching. Practical experience FLD introduced by Keeler [30]; Goodwin [31]; Hecker [32] and experimental tests by Arzin [33]; Ghosh [34]; Painter [35] have demonstrated that thin sheets subjected to positive biaxial tension can fail by localized necking criterion [36].

Efforts to provide closed-form, exact models have been under way since publication of one of the earliest studies by Chung and Swift [37]. This study was followed by others [38-44].

In several of these works, however, approximations found in the description of a large deformation plasticity could influence the results, particularly for more complex, sharp tool geometries. Comparison with experimental results is often missing for important process parameters.

In this study, the MARC program [45] implemented rigid-plastic flow analysis capability, in which elastic incremental strains are assumed negligible compared to plastic incremental strains in the fully developed plastic region.

3.2 General Organisation of MARC System

The MARC system consists of the following programs: MARC and MENTAT. These programs together with: (a) generate geometric information that defines structure (MARC and MENTAT); (b) analyse structure (MARC); and (c) graphically depict the results (MARC and MENTAT).

3.3 Rigid-plastic FEM

The principle of virtual work describes the equilibrium equation and boundary conditions. Suppose that the shape of the surface and the distribution of the effective strain are given or have been determined already at a time t_o. The variation of internal energy in the sheet metal at time $t_o + \delta t$ is represented as follows [46].

$$\delta W = \int \sigma_{ij} \delta \varepsilon_{ij} dV \tag{4}$$

where σ_{ij} is the second Piola-Kirchhoff stress tensor and ε_{ij} is the Lagrangian strain tensor. The second Piola-Kirchhoff stress tensor is turned into the Cauchy stress for incompressible material in the convected coordinate system. When the sheet metal in the bending condition, the strain tensor can be considered to consist of two terms:

$$\varepsilon_{ij} = \varepsilon_{ij}^{m} + \varepsilon_{ij}^{b} \tag{5}$$

where ε_{ij}^{m} is the membrane strain and ε_{ij}^{b} is the bending strain.

The strain due to bending can be expressed in terms of the curvature. Thus, internal energy term can be expressed as:

$$\delta W = \int_A \sigma_{ij}^m \delta \varepsilon_{ij}^m t dA + \int_A M_y \delta \rho_y dA \tag{6}$$

where M_y is the bending moment and ρ_y is the radius of curvature.

With the use of the natural convected coordinate system, the derived virtual energy formulation is more easily transformed into a form of a FE approximation. After the algebraic manipulation, the membrane energy term in Eq. (6) is expressed as:

$$\delta W^m = \int_A \sigma_{ij}^m \delta \varepsilon_{ij}^m t dA = \int_A \bar{\sigma} \delta(\Delta \bar{\varepsilon}) t dA = \delta U^T Q^b(\bar{U}) \tag{7}$$

Also the bending energy term in Eq. (6) can be derived as:

$$\delta W^b = \int_A M_1 \delta(\Delta \rho_1) dA + \int_A M_2 \delta(\Delta \rho_2) dA = \delta U^T Q^b(\bar{U}) \tag{8}$$

where $\rho_1 = (W_i^1 - W_i^2)/L_i$, L_i is the distance between the centers of two neighboring elements and W_i^1, W_i^2 are the derivatives of the normal displacements in the direction normal to the boundary respectively [47].

By eliminating the virtual displacement δU, the variational expression of Eq.(6) is approximated to the following algebraic equation:

$$Q^m(U) + Q^b(U) = F \tag{9}$$

which is a nonlinear function of U. In Eq. (9), F is the external force vector. This nonlinear algebraic equation is solved iteratively by Newton-Raphson method.

4. NUMERICAL CALCULATION

4.1 Deep Drawing Simulation of a Square Box

The forming analysis was performed with MARC package using rigid-plastic flow method. The tooling was converted from Pro/Engineer system into IGES formats and meshed pre-processing MENTAT program. Fig. 2 shows the profile of the die, punch head, blankholder, the initial shape and FE mesh.

4.1.1 Geometry

The sheet was made up of 1900 four-node shell element type 75, initially square with round corner. Element 75 is a thick shell element which may also be used to simulate thin shells. The initial shell thickness is 0.85 mm. Four layers are used through the thickness of the shell. The punch was square shape 40x40 mm. The punch had a constant velocity of 25 mms^{-1}. The analysis was carried out with 380 increments and AUTO LOAD option. The total punch travel is 40 mm.

4.1.2 Boundary Conditions

One-quarter of the geometry is used due to symmetry. The appropriate nodal constrains are applied in the global X, Y directions to impose symmetry.

4.1.3 Contact

Contact option declares that there are four bodies in contact with Coulomb friction between them. The first body is the blank, the second body is the punch, the third body is the die, and the last body is the blankholder. The tools were modeled as rigid and coefficient of friction, μ=0.11 was associated with each tool. The contact tolerance distance is 0.02 mm. The rigid surfaces are offset from the blank by half of thickness of blank, because the contact algorithm takes into account the shell thickness.

4.2 Deep Drawing of a Circular Cup

Performed simulation of the stamping process circular blank with flat-headed punch, and typical for forming operations punch/die clearance. Numerous applications were carried out using dynamic explicit method of FEM simulation.

4.2.1 Geometry

A circular blank was modeled by 1460 shell FE (element 75). The initial shell thickness was 0.85 mm. Four layers are used through the thickness of the shell. The die was fixed in space. Fig.3 shows the profile of the die, punch head, blankholder, and FE mesh.

4.2.2 Loading

The explicit analysis was carried out with 20,000 increments, where the mass was scaled by factor 100,000. The punch velocity was 50 mm s^{-1}. The AUTO LOAD option was applied and total punch travel is 40 mm.

4.2.3 Boundary Conditions

One-quarter of the axisymmetric geometry is used due to symmetry for easier visualisation. Boundary conditions are used to enforce symmetry about the X, Y-axes.

4.2.4 Contact

The punch, die and blankholder are modeled as rigid bodies. The Coulomb friction model with a constant coefficient of friction, $\mu = 0.11$ was applied. The contact tolerance distance is 0.02 mm.

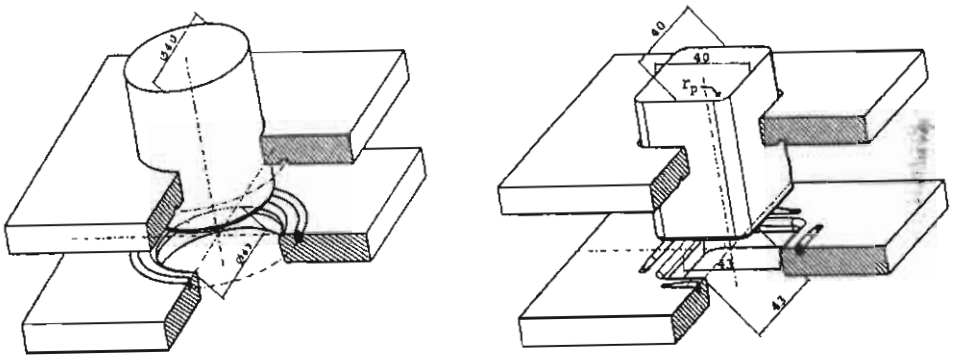

(a) (b)

Figure 1. Deep drawing tool geometry used in circular punch (a) and square punch r_d = 6 mm and r_p= 8 mm.

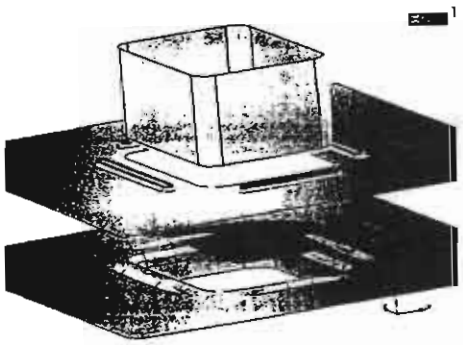

Figure 2. Simulation model for square cup.

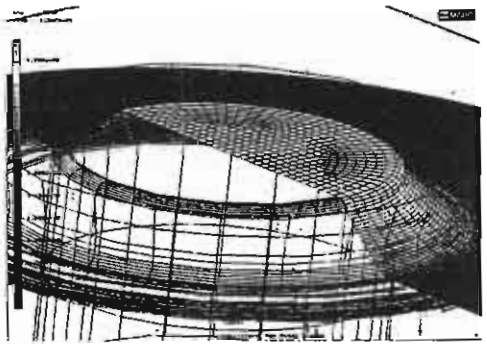

Figure 3. Simulation model for circular cup.

5.RESULTS AND DISCUSSION

The model described above was implemented using MARC FE package programs and the following results were obtained.

5.1 Strain and Stress Forming Limit Diagrams of Circular and Square Cups

Forming limit diagram (FLD) and forming limit stress diagram (FLSD) obtained from the deformed square cup in Fig. 4 are shown in Figs. 5 and 6 for DDQS and AL sheets respectively.

The new orthotropic damage model [20] for localized necking is employed to predict the FLD. The as-received materials are assumed to suffer no initial damage prior to load application. The external load increment along principal direction 1 is 10 N, corresponding to an initial principal stress increment $\Delta\sigma_1 = 10$ MPa. For a particular strain path β, stress ratio $\alpha = \Delta\sigma_2 / \Delta\sigma_1$ (although β is assumed to be a constant, α is no longer constant due to damage effect). The values of σ_1 and σ_2 for initial yield are first obtained. This is followed by the calculation of the stress increments $\Delta\sigma_1$ and $\Delta\sigma_2$ based on the current element geometry and α. The elastic strain is assumed to be negligible.

Strains for diffuse necking, localized necking and final rupture are obtained when their respective instability criteria are satisfied [48]. The predicted diffuse necking, localized necking and rupture diagrams for AL sheet is shown in Fig. 7, while a comparison between the predicted FLD (which is based on localized necking) results and experimental data is shown in Fig.8. From this figure, it can be seen that good agreement between numerical and experiment exists.

In Fig.9, the predicted FLD results from different methods are compared. The figure shows that most methods predict higher FLD's compared with that based on the damage model for localized necking. In addition, with the damage instability criteria, the diffuse necking curve and the localized necking curve are shown to intersect at the same point at plane strain when β=0 (i.e. ε_2=0) as would be expected physically and experimentally. This important phenomenon is not often observed in the FLD predicted using the conventional approaches.

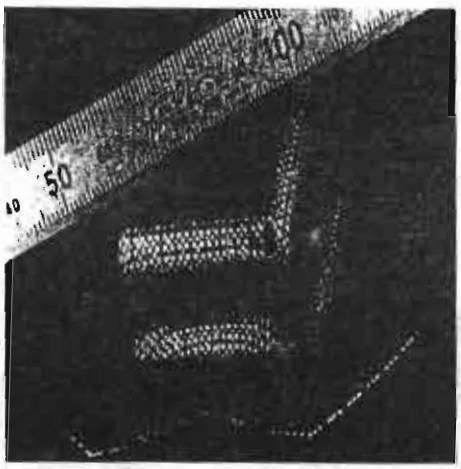

Figure 4. Deformed square cup.

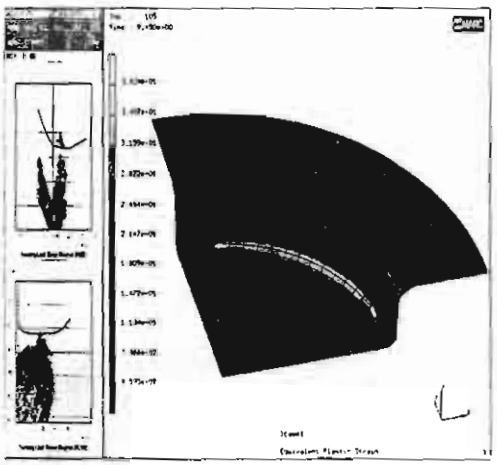

Figure 5. Numerical FLD and FLSD of DDQS circular sheet.

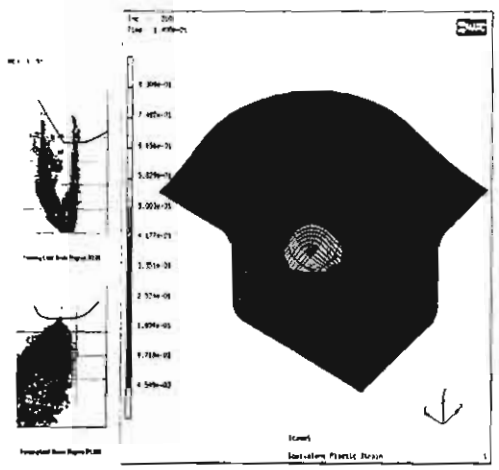

Figure 6. Numerical FLD and FLSD of AL square sheet.

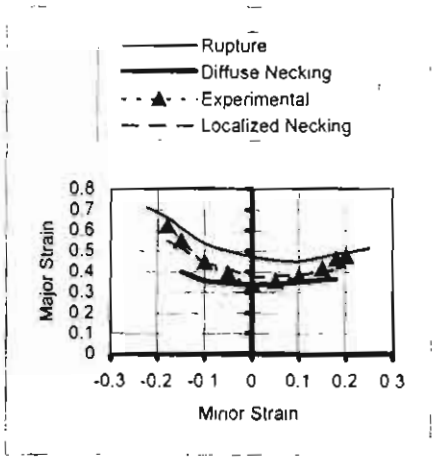

Figure 7. The predicted FLD of AL alloy.

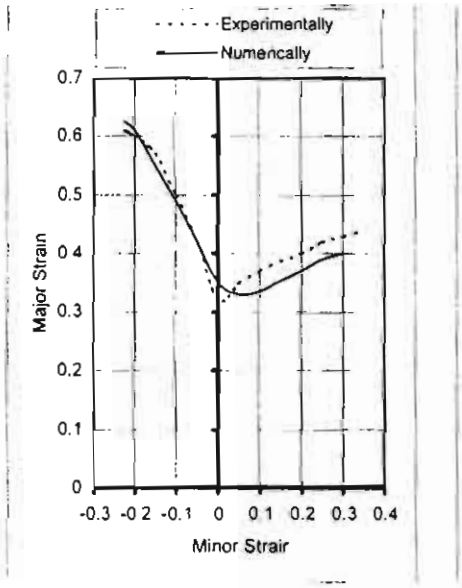

Figure 8. Comparison of experimental FLD and predicted FLD of AL alloy.

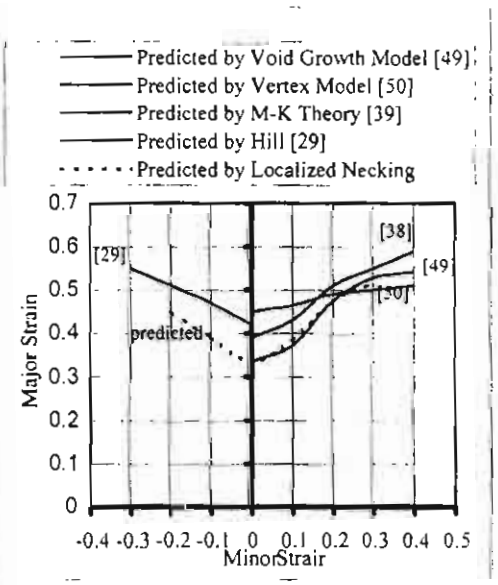

Figure 9. A comparison of the FLD's of AL alloy.

5.2 Thickness Distribution

Fig.10 shows the numerical thickness distribution of the tested materials for circular cup. In Fig. 11 numerical predicted and experimental strain distributions are compared at a common punch depth. The experimental radial strain ε_r is represented by filled circles, the experimental circumferential strain ε_θ by open circles, the experimental thickness strain ε_t by open triangle, and the corresponding numerically determined strains, by solid lines. Both experimental and numerical strain distributions show the same basic features. At the circular punch head (original radial coordinate 0-17 mm), ε_r and

ε_θ are small, similar and positive while ε_r decreases toward small negative value. At the punch profile radius (original radial coordinate 17-25 mm), ε_r gradually increases while ε_θ decreases toward large negative values. In the wall of the cup (original radial coordinate 25-approximately 35 mm). ε_r increases to a maximum of the die edge and ε_θ decreases to a minimum at the die edge. In the flange of the cup. ε_r again decreases while ε_θ increases. In Fig. 11, it can be seen that good agreement between experimental and calculation values are obtained.

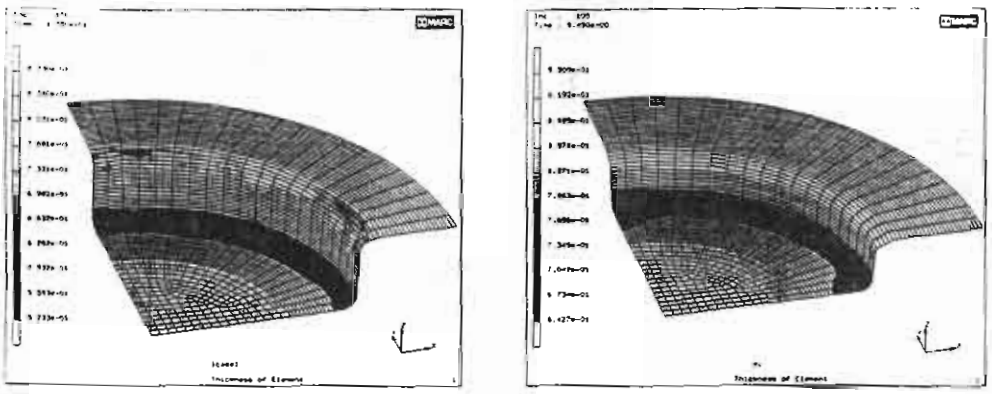

AL alloy DDQS

Figure 10 Numerical thickness distribution.

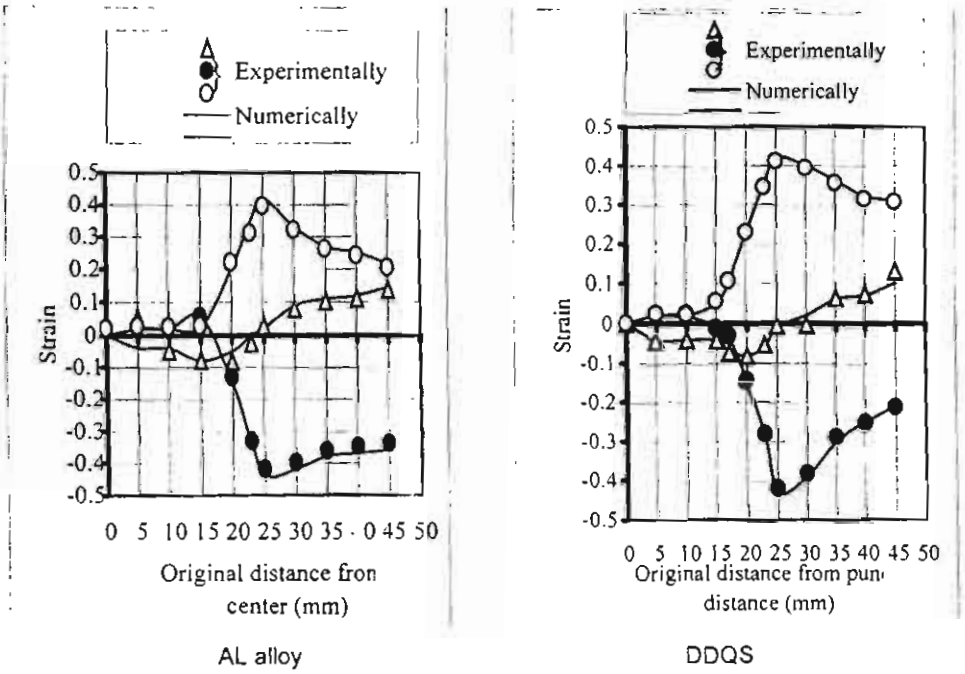

AL alloy DDQS

Figure 11. Comparison between predicted and experimental thickness distribution.ε_r is radial strain, ε_θ is circumferential strain, and ε_t is thickness strain.

6. CONCLUSIONS

A numerical model based on rigid-plastic method has been proposed in this paper to predict the forming limit diagram (FLD), forming limit stress diagram (FLSD) and thickness distribution for a deep drawing quality steel (DDQS) and aluminium alloy (AL). The model took into consideration the planar anisotropic value, the material properties, blank shape, and coefficient of friction. The model implemented uses the MARC K7.1 FE package. For comparison purpose, various results regarding the FLD and FLSD predictions were calculated using the FE computer program described. These results were then compared with experimental measurements. The comparison indicated that the numerical model is capable of predicting strain and stress distributions not only qualitatively but also quantitatively with good agreement.

Based on this study, the following remarks are drawn.

1. The rigid-plastic method reducing the total computation time compared with the explicit method.
2. The inertia effect in explicit analysis plays an important role in influencing the results.
3. The implicit method treats the sheet forming without changing its physic.

Acknowledgements

The author wishes to thank Professor Dr . Eng. J. Gronostajski (D.Sc.) for valuable guidance during the work reported in this paper. Thanks are also due to Dr. Eng. Z. Zimniak for his help in numerical computation, and to the staff of the workshop of the Metal Forming Department, Institute of Machine Building Technology, Technical University of Wrocław, Poland.

REFERENCES

[1] A. Barata Da Rocha, et. al: Prediction of the forming limit diagrams of anisotropic sheets in linear and non-linear loading, *Mater. Sci. Eng.*., Vol.68, p.151, 1985.

[2]G.Beveridge and R.Schechter, *Optimization: Theory and practice*, McGraw-Hill Book Company, New York City, NY. 1970.

[3] M. Gotoh and F. Ishise: A finite element analysis of rigid-plastic deformation of the flange in a deep drawing process based on a fourth-degree yield function, *Int. J. Mech. Sci.*, 20, p. 423, 1978.

[4] H. Iseki and T. Murota: Analysis of deep drawing of non-axisymmetric cups by the finite element method, *Proc. Ist ICTP*, Tokyo, p. 678. 1984.

[5] R. Sowerby, et. al: The development of computer aids for sheet metal stampings in CAD/CAM and FEM in metal working, Ghosh,S.K. and Niku-Lair,A., Ed., *Pergamon Press*, p. 187, 1988.

[6]R.H.wagoner,et. al: Forming limit diagrams: Concepts, Methods, and Applications. TMS, *Warrendale, Pennsylvania*,USA, 1989.

[7] R.Sowerby, et. al: The modeling of sheet metal stamping, *Int. J. Mech. Sci.*, 28, p. 415, 1986.

[8] Y. Q. Guo, et. al: Finite element procedures for strain estimations of sheet metal forming parts, *Int. J. Numer. Methods ENG.*, 30, p. 1385, 1990.

[9] J. H. Vogel, et. al: An integration process design method for sheet material forming, *15th Biennial Con. IDDRG*, Dearborn, Michigan, USA, p. 265, 1988.

[10] K. Lange, et. al: Application of an elasto-plastic finite element code to the simulation of sheet metal forming processes, *J. Mater. Process. Tech.*, Vol. 27, p. 239, 1991.

[11] H. Y. Jiang and D. Lee: Numerical simulation of sheet metal forming process based on large deformation sheet elements. *Proc. NUMIFORM'92*, p. 485, 1992.

[12] T. B. Stoughton: Finite element modelling of 1008 AK sheet steel stretched over a rectangular punch with bending effect, Computer Modelling of the forming process-Theory, Verification and Application, Wang, N.M., and Tang, S. C., eds., AIME, 1985.

[13] A. P. Karafillis and M.C. Boyce: On the modeling of contact in finite element analysis of forming processes, *Numerical Methods in Industrial Forming Processes*, Balkema, Rotterdam, 1992.

[14] S. Badrinarayanan and S.N. Zabaras: Perform design in metal forming, *Proc. NUMIFORM'95*, p. 533, 1995.

[15] L. Fourment and J. L. Chenot: Optimal design for non-steady state metal forming process-Part I Shape optimization method, *Int. J. Numer Methods. Eng.*, Vol. 39, 1996 p. 33.

1. Introduction

Fouling of heat transfer surfaces is one of the most important problems in heat transfer equipment. Fouling can occur on any fluid-solid interface and has adverse effects on the unit performance, in which it leads to decrease production, efficiency, and life of the unit. On the other hand, fouling leads to increase both of the capital and operating costs. Overcoming fouling is therefore essential for technical and economic considerations. Solution of the problem requires a better understanding of the physical processes causing fouling.

According to many investigators, fouling can be considered as the single most unknown factor in the design of the industrial equipment. This situation exists despite the wealth of operating experience accumulated over the years and accumulation of fouling literature. This lack of understanding almost reflects the complex nature of the phenomenon by which the fouling occurs in industrial equipment. The wide range of process streams and operating conditions present in industry tends to make most fouling situation unique, thus rendering a general analysis of the problem is difficult.

The interest in fouling research has increased greatly over the past twenty years. Many efforts were paid to decrease and prevent fouling, develop cleaning methods, and overcome the fouling effects. Some success has been obtained in every goal, but up to date, there is no clear and sufficient way that can be used to mitigate the fouling or the fouling effects. Some of the earliest papers on fouling appeared in the early 1920's and there were few additions to the literature up to 1960. Fouling was one of the major areas selected for investigation by the Heat Transfer Research Incorporation, (HTRI), in 1960. It was described as "the major unresolved problem in heat transfer". HTRI developed a measurement technique and obtained a large amount of data on the fouling characteristics of cooling tower water, seawater, and crude oil. Since 1960 there has been a significant increase in the literature on fouling and a considerable increase of interest in the subject. A review by Epstein (1983) contained over 150 references on fouling has been published between 1960 and 1977.

The International Conference on the "Fouling of heat transfer equipment" held in August 1979, objected to critically assess the present status of fouling research, review methods for the prediction of fouling, and identify the important directions for future research. In this conference, it was demonstrated that the basic mechanisms of many types of fouling are similar and that the theories used to explain one type of fouling might be indeed by used as a basis to explain other types.

Many investigators have studied the fouling phenomenon theoretically and experimentally. Kern and Seaton . 1966, have cited the first and the pioneer mathematical model for surface fouling. They stated that the fouling rate could be estimated as the difference between the deposition and removal rates. Also, they proposed that the deposition rate is proportional to the product of foulant concentration and flow rate whereas the removal rate is proportional to the shear stress and the instantaneous thickness of the deposit. In this model, if the removal term is small and always less than the deposition term, the fouling factor may increase indefinitely until the flow path is plugged. If the removal term is significant, a point may be reached where deposition and removal rates become equal and the fouling reaches asymptote value which is called asymptotic fouling factor.

Taborek, et.al., 1972, introduced the water characterization factor to the deposition term to account for the effect of water quality. They expressed the deposition rate by the so-called *Arrhenius* type equation. The removal term was postulated to be a function of shear stress, deposit thickness, and bonding strength of the deposit.

Watkinson, et.al., 1974, obtained a set of experimental fouling-time curves and compared their results against the fouling model proposed by Kern and Seaton, 1966. It was

found that, the asymptotic fouling resistance was inversely proportional to the squared mass flow rate. Also it was found that, the initial fouling rate was inversely proportional to the mass flow rate and dependent exponentially on the initial wall temperature. They proposed a deposition term which equal the product of the foulant mass flux normal to the surface, j, and the sticking probability, p, which in turn is proportional to the adhesive force binding a particle to the surface, and inversely proportional to the hydrodynamic forces at the interface. The proposed removal term was formulated similar to that of Kern and Seaton.

Beal, 1978, described a new and potentially promising method for predicting the deposition of particles entrained in turbulent flow as a function of concentration gradient in normal direction times the sum of molecular and eddy diffusivity.

Watkinson, 1980, reported experimentally the effect of fluid velocity on the asymptotic fouling resistance for three different operating foulants and obtained a correlation for each.

Reitzer, 1981, considered the rate of scale formation in tubular heat exchangers. He assumed that fouling factor is linearly dependent on time, therefore no asymptotic fouling had been reached. He concluded that an additional removal mechanism is required to physically represent a complete fouling model.

Knudsen, 1986, composed the fouling models due to Kern and Seaton, 1966, and Taborek, et.al., 1972, and proposed a deposition - removal model based on the *Arrhenious* theory for both asymptotic factor and time constant.

Epstein, 1988, proposed a simple model to describe the asymptotic fouling type. He assumed that the deposition rate is constant, where the removal rate is proportional to the thickness of the deposited layer.

Recently, Webb and Li, 2000, investigated the effect of internal tube enhancement on the fouling rate for cooling tower water. They found that the enhancement parameters such as helix angle and number of starts have significant effects on the fouling mechanism. It is observed that, fouling increases as the number of starts and helix angle increases.

Li and Webb, 2000, extended their pervious work to study the effect of different fouling types. A comparison between pure particulate fouling and combined precipitation and particulate fouling had been carried out. They found that, the fouling resistance due to pure particulate fouling is less than that due to the combined precipitation and particulate fouling.

Forster and Bohnet, 2000, analyzed the influence of interfacial energies between two materials on adhesion based on van der Waals and hydrophobic interactions. They introduced a new anti-fouling strategy dealing with molecular interactions at the interface crystal /heat transfer surface to reduce the corresponding adhesive strength favoring the removal process due to the wall shear stress.

Schwarz, 2001, reported a long-term evolution of heat transfer performance of steam generators in many Siemens pressurized water reactors. It is concluded that, the iron deposition has drastically reduced and consequently, the fouling increase has almost stopped. This reduction occurred in all plants that have started under phosphate treatment for a long term of operation and their feed water chemistry have been converted to H-AVT treatment (all volatile treatment with hydrazine dosing to assure high pH-values). In plants, which operate under H-AVT from the beginning, no significant fouling factor increase has been observed. Hence, H-AVT treatment is preferred for feed water chemistry, not only from a corrosion prevention point of view but also from a heat transfer performance as well.

Kim, *et al*, 2001, investigated the effect of electronic anti-fouling (EAF) technology on fouling mitigation in a heat exchanger in an open cooling tower systems. They found that, the fouling resistance with EAF treatment was about 70% less than that without EAF treatment, at the end of 270-hr tests.

In the light of the above review, the effect of dynamic aspects of flow is not considered. In the present work, the effect of flow oscillation on the fouling parameters in pipe flow is investigated. A modification of Kern and Seaton model has been introduced to assess the dynamic effects due to flow oscillation.

2. Computational Methodology

2.1. Governing Equations

The momentum equation for unsteady, incompressible, fully developed oscillating flow in a circular tube has been reduced to;

$$\rho\frac{\partial u}{\partial t}=-\frac{dp}{dz}+\mu\left(\frac{\partial^2 u}{\partial r^2}+\frac{1}{r}\frac{\partial u}{\partial r}\right) \tag{1}$$

In which the given oscillating pressure gradient is given by;

$$\frac{dp}{dz}=-\rho K e^{i\omega t} \tag{2}$$

The solution of Eq.(1) subjected to the harmonic pressure gradient of Eq.(2) along with the non-slip boundary conditions at the tube wall, yields the oscillating velocity distribution. This velocity distribution can be expressed in terms of the Bessel function of the first kind of order zero in radial direction, and has a harmonic dependence in time as follows:

$$u(r,t)=\frac{K}{i\omega}e^{i\omega t}\left\{1-\frac{J_o\left(r\sqrt{-i\omega/\nu}\right)}{J_o\left(r_o\sqrt{-i\omega/\nu}\right)}\right\} \tag{3}$$

The associated shear stress distribution can be found upon differentiation of Eq.(3) as;

$$\tau(r,t)=\rho\frac{K}{\sqrt{-i\omega/\nu}}e^{i\omega t}\left\{\frac{J_1\left(r\sqrt{-i\omega/\nu}\right)}{J_o\left(r_o\sqrt{-i\omega/\nu}\right)}\right\} \tag{4}$$

Following Kern and Seaton postulate, the fouling model, can be expressed as;

$$\frac{dx}{dt}=k_1\ Q(t)\ c-k_2\ \tau_w(t)x \tag{5}$$

The above equations have been normalized by the following reference parameters: for length, r_o (pipe radius); velocity, $u_{max.s}=\frac{r_o^2}{4\nu}K_s$ (steady state centerline velocity); and for time, $\frac{r_o^2}{\nu}$

The derived reference parameters are: circular frequency, $\frac{\nu}{r_o^2}$ and shear stress, $\frac{1}{2}\rho\ u^2_{max}$

Upon normalizing each variable with its corresponding reference parameter, a system of non-dimensional equations is obtained as follows:

(from now on, each symbol represents a non-dimensional variable)

$$u(r,t)=-\frac{4i}{\omega}\frac{K}{K_s}e^{i\omega t}\left\{1-\frac{J_o\left(r\sqrt{-i\omega}\right)}{J_o\left(\sqrt{-i\omega}\right)}\right\} \tag{6}$$

$$\tau(r,t)=\frac{-16}{\sqrt{-i\omega}}\frac{1}{\mathrm{Re}_d}\frac{K}{K_s}e^{i\omega t}\left\{\frac{J_1\left(r\sqrt{-i\omega}\right)}{J_o\left(\sqrt{-i\omega}\right)}\right\} \tag{7}$$

$$\tau_w(t) = \frac{16}{\sqrt{-i\omega}} \frac{1}{\mathrm{Re}_d} \frac{K}{K_s} e^{i\omega t} \left\{ \frac{J_1\left(\sqrt{-i\omega}\right)}{J_o\left(\sqrt{-i\omega}\right)} \right\} \qquad (8)$$

From the above review, and following Kern and Seaton model, the fouling rate is the outcome of two essential processes. The first is the deposition process, which is proportional to the amount of flow rate and the concentration of foulant material in the stream. The second is the removal process which is proportional to the wall shear stress and the fouling thickness x. In case of steady flow, in which both flow rate and wall shear stress are approximately invariant with the fouling thickness x, it can be easily found that the fouling reaches an asymptotic value x^*.

As it is well known, the effect of the dynamic forces is greater than that of the corresponding steady state. Therefore, to enhance the removal force, a dynamic flow application is sought. On the other hand, the dynamic flow will reduce the foulant settlement on the surface. Subsequently, the overall dynamic flow effects are in favor of fouling reduction. However, the operations of industrial equipment are designed on steady flow state, a marginal dynamic flow could be tolerated. In fact, the notion of steady state operation is quite an assumption rather than a reality.

In the present work, the dynamic aspects that affect the fouling mechanism are embedded in Kern and Seaton Model by replacing the steady state flow rate and shear stress by their instantaneous value from Eqs.(6 and 8). The other dynamic effects lie in the proportionality constants k_1 and k_2. In fact, it is assumed that the major effect of oscillating flow on the fouling is the enhancement of these constants in favor of minimizing the deposition term and maximizing the removal term. This dynamic effect is taken to be the ratio of the maximum amplitude of the wall shear stress to that of the steady flow. This ratio is always greater than unity for any dynamic flow parameters.

From the above discussion the dynamic fouling model due to the flow oscillation can be written as;

$$\frac{dx}{dt} = k_1 \, Q(t) \, \mathrm{Re}_d \, c - k_2 \, \tau_w(t) \mathrm{Re}_d^{\,2} \, x \qquad (9)$$

Equations (6 to 9) have been coded in a FORTRAN program and the results are obtained at each time step for each harmonic. For any given periodic function representing the pressure gradient, a Fourier transform is used to get its frequency spectrum and Eqs.(6 to 9) have been solved for each harmonic component and added to yield the equivalent solution.

Five different periodic pressure wave forms namely sine, step, triangular, trapezoidal, and saw teeth, have been used in this investigation to study the effect of dynamic flow parameters such as: dynamic pressure amplitude, frequeney and Reynolds number on fouling characteristics.

3. Results and Discussion

A parametric computational study has been carried out to study the effect of oscillating flow parameters such as pressure amplitude, frequency, and wave form on the fouling rate and its asymptotic value. The effect of Reynolds number on the dynamic fouling characteristics has been investigated as well. All parameters are represented in a non-dimensional forms.

A sample of the output results is displayed in Fig.(1). It can be seen that the wall shear stress is lagging the given pressure sine wave by a phase of about $\pi/4$ where the flow rate is lagging by about $\pi/2$. This can be drawn from Eqs.(6 and 8) in which the time phase angles are

represented by the argument of the complex amplitude of both velocity and wall shear stress. These angles are the arguments of i and $i^{3/4}$ for both velocity (flow rate) and wall shear stress.

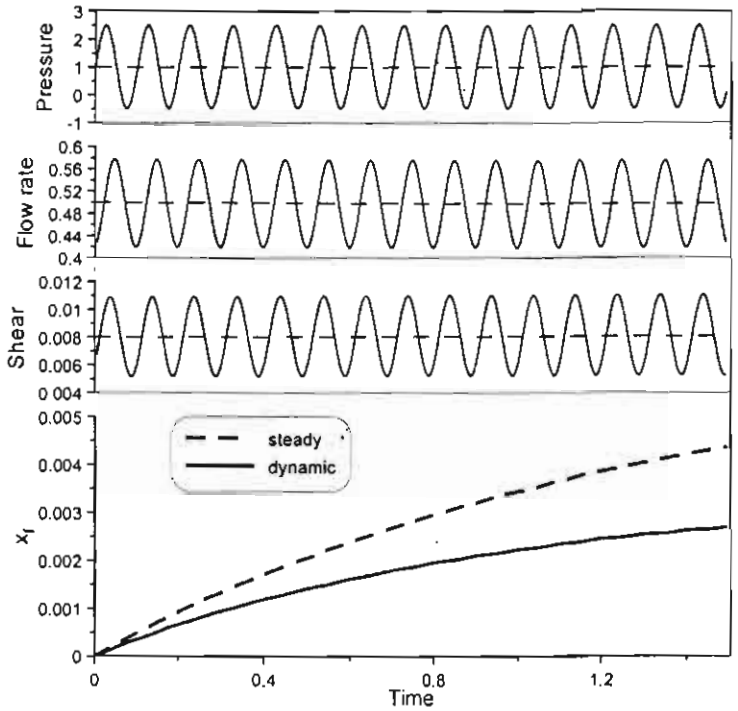

Fig.(1) Dynamic flow parameters for pressure sine wave form, at $f=10$, $K/Ks = 1.5$

The fouling thickness, x for both dynamic and steady flow are also displayed. It is clearly shown that, the dynamic fouling thickness and fouling rate are reasonably smaller than their corresponding steady values. This could prove that, the oscillating flow, in fact, alleviate the fouling problem. The asymptotic value of fouling for both dynamic and steady flow have not reached in this plot because of the non dimensional run time is small just to show the details of the dynamic flow parameters.

In Fig.(2), the pressure wave form and fouling curves for the other wave forms are illustrated. From this figure it is seen that, the dynamic fouling thickness and rate are less than their corresponding steady values for all wave forms. Figure (3) has been illustrated to show the effect of pressure wave form on the fouling parameters. In Fig.(3.a), the result of all five wave forms is summarized and their asymptotic trend is clearly displayed. In this figure the run time is long enough to reach the asymptotic fouling thickness x^*. A bar chart representing the asymptotic values, shown in Fig.(3.b), illustrates that the best shape is the step wave form and the poorest one is the saw teeth.

All test runs from now on will be done with enough time such that the asymptotic fouling thickness has been reached.

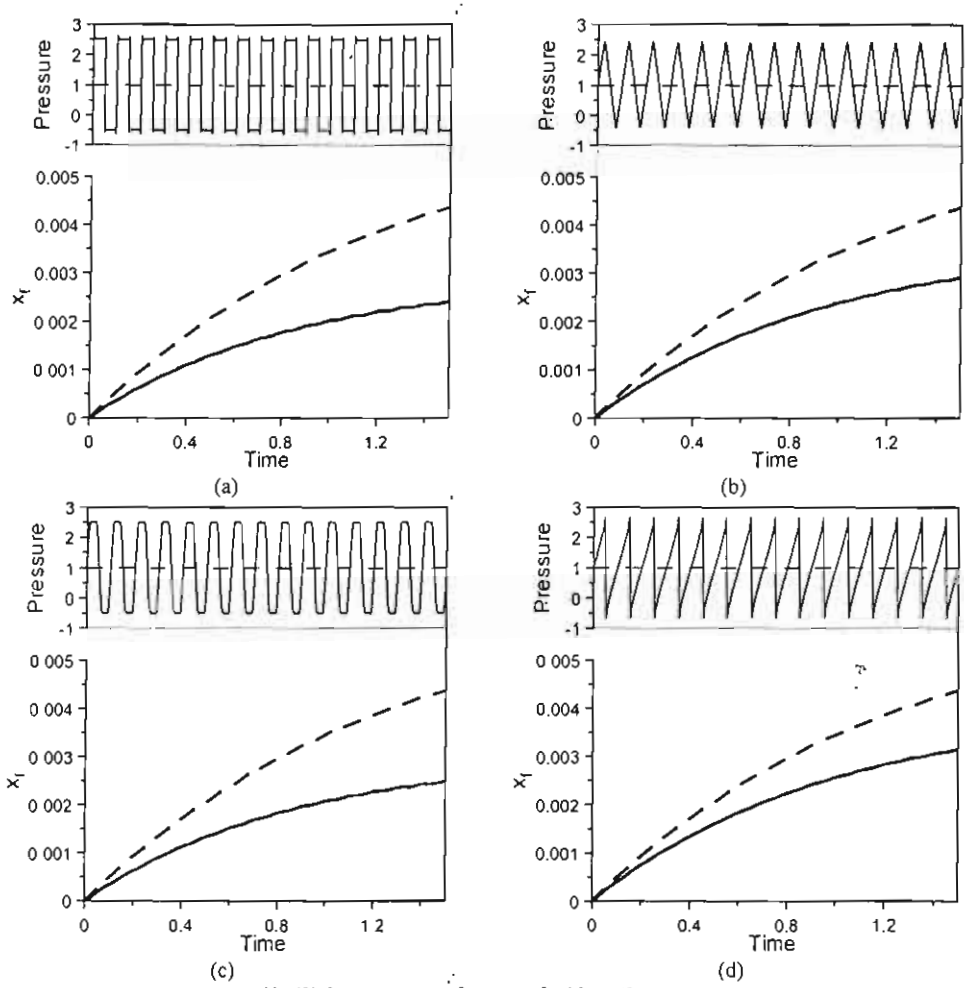

Fig.(2) Pressure wave form, at $f = 10$, $K/Ks = 1.5$
(a) step, (b) triangular, (c) trapezoidal, and (d) saw teeth
—— dynamic ---- steady

To investigate the effect of pressure wave amplitude on the fouling parameters, Fig.(4) has been illustrated for the sine wave shape. From this figure, it is seen that, the wave amplitude has a drastically effect on the fouling rate and its asymptotic value. The fouling rate and the asymptotic value are decreased by increasing the wave amplitude, that is due to increase of dynamic effects which increase the removal rate and may decrease the deposition one. From Fig.(4.b), it can be drawn that, the rate of fouling reduction is much pronounced at low amplitudes than at higher amplitudes. This could be beneficial in the industrial applications whenever any small marginal flow oscillation can be tolerated.

Figure (5) shows the effect of pressure wave frequency on the fouling parameters. From the figure, it can be seen that, increasing the wave frequency increases the fouling rate and the asymptotic value. Increasing the wave frequency decreases the dynamic effects. In the limit, for a very high frequency the flow approaches the steady state condition. From Fig.(5.b), it can be drawn that the wave frequency has a very limited effect on the fouling reduction at high frequencies.

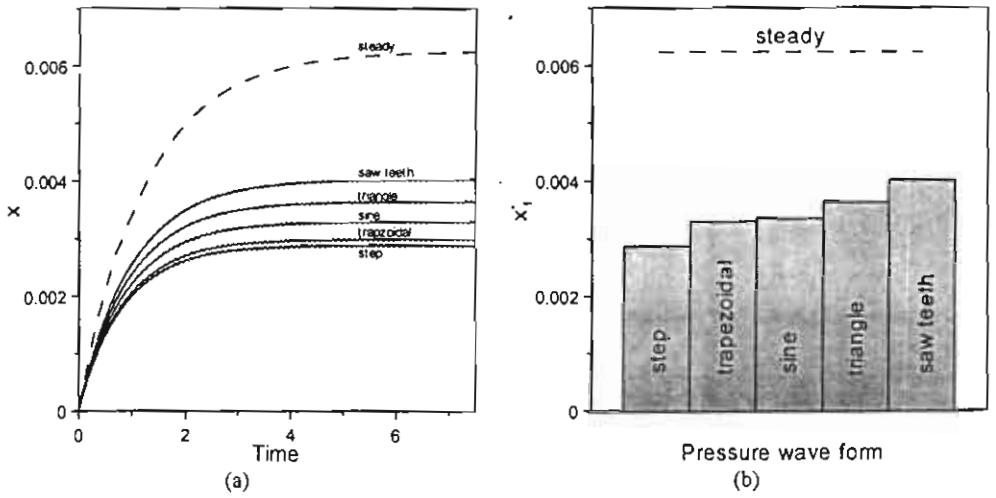

Fig.(3) Effect of pressure wave form on the fouling parameters, for $f=10$, $K/Ks = 1.5$

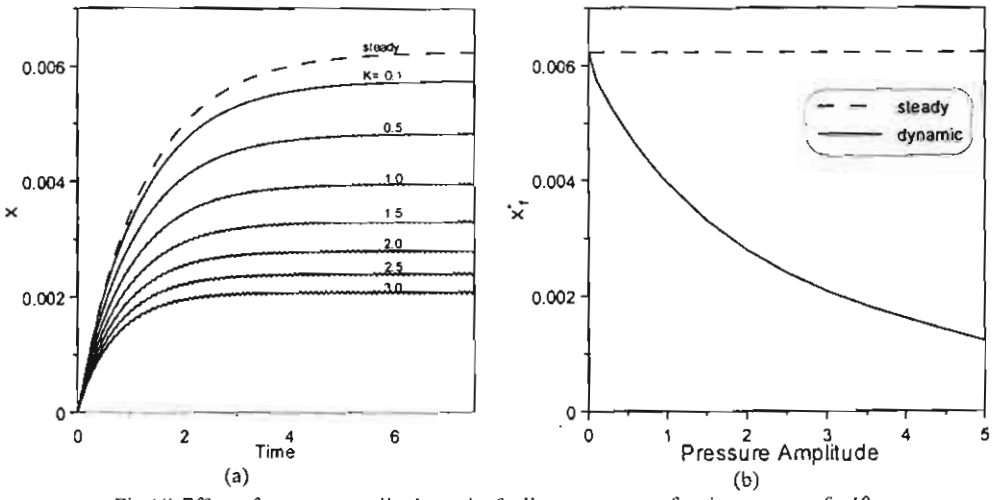

Fig.(4) Effect of pressure amplitude on the fouling parameters, for sine wave at $f=10$

Figure (6) has been presented to show the effect of flow Reynolds number on the fouling parameters. For a given pressure wave amplitude and frequency, the major effect of Reynolds number is decreasing the fouling rate or time constant as Reynolds number increase as shown in Fig.(6a). On the other hand, Reynolds number has no effect on the asymptotic fouling thickness. In fact, the change of the Reynolds number does not affect the asymptotic fouling thickness because of the flow and fouling model in this study are based on laminar flow theory. The corresponding time constant t_c is shown in Fig.(6b). From this figure the time constant for both dynamic and steady conditions are quite different at low Reynolds number. and approach the same small value at high Reynolds number. This could be stated as the dynamic flow fouling is quite decelerated at low Reynolds rather than at high values.

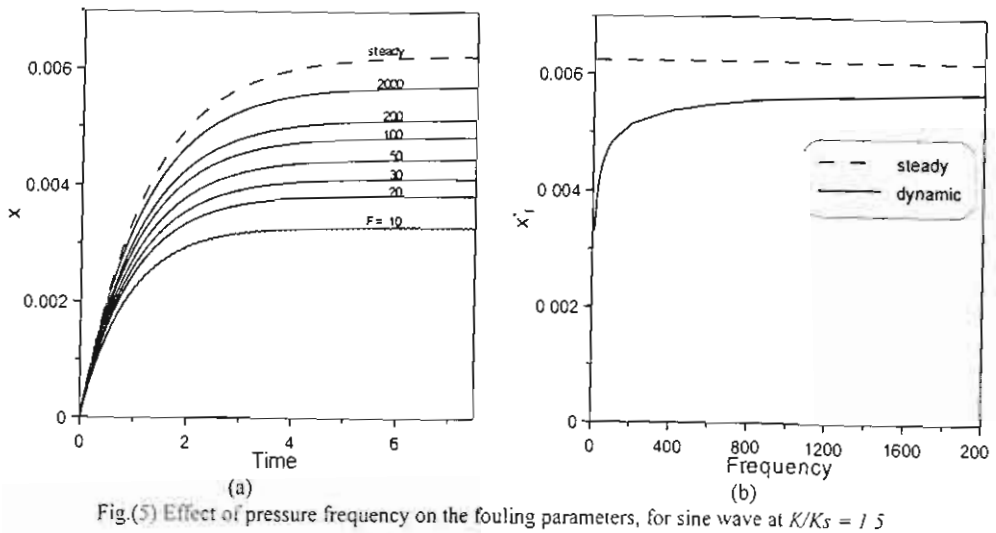

Fig.(5) Effect of pressure frequency on the fouling parameters, for sine wave at $K/Ks = 1.5$

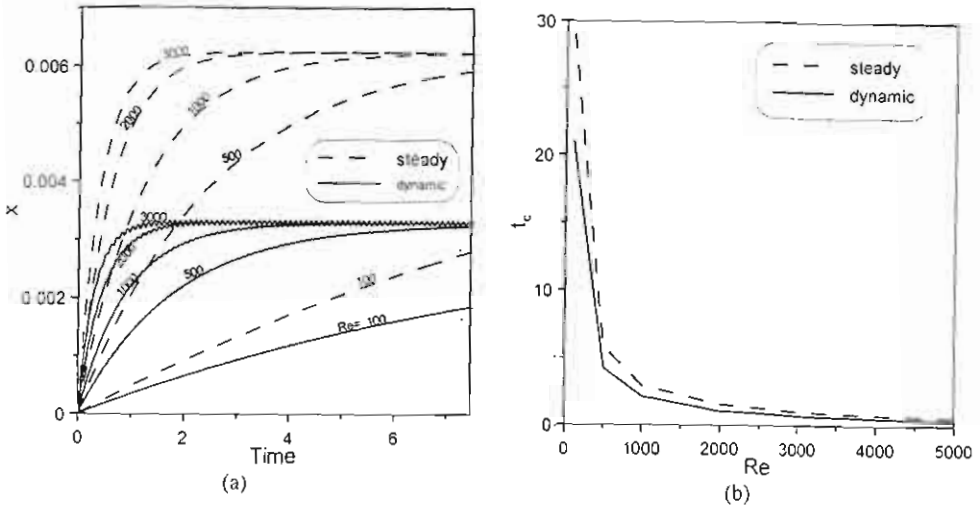

Fig.(6) Effect of Reynolds number on the fouling parameters, for sine wave at $f = 10$, $K/Ks = 1.5$

4. Conclusions and Recommendations

A fouling model accommodating the effect of flow dynamics has been developed. The effect of flow oscillation parameters has been investigated. However, the operation of industrial equipment usually, designed with the notion of steady state operation, a small marginal dynamics can not be avoided. In the light of this fact and the aforementioned discussion, a reasonable fouling reduction has been found.

For all investigated pressure gradient wave forms, It is found that the fouling problem has been alleviated. The step wave form has the greatest effect to mitigate the fouling, where the saw teeth wave form has the smallest effect. A typical reduction is found to be *54%* for step wave form and *34%* for the saw teeth.

An oscillating pressure gradient of sine wave form has been used to test the dynamic flow parameters on the fouling in flow inside tube. The effect of pressure oscillation

amplitude is found to have a pronounced fouling reduction. At very low marginal amplitude, the fouling is quite mitigated. A great reduction is found to be *36%* for pressure gradient amplitude ratio as high as one and *8%* for a value as less as *0.1*.

The pressure wave frequency has a quite effect on the fouling reduction at low wave frequencies, where this effect diminishes as the frequency increases enough such that the steady state is reached. The reduction is found to be *46%* for frequency of *10* and *22%* for *100*.

The increase in flow Reynolds number reduces the fouling rate but has no effect on the asymptotic fouling thickness.

References

Beal, S.K., 1978, "Correlation for the sticking probability and erosion of particles," J. Aerosol Sci., Vol. 9, pp. 455-461.

Schwarz, T., 2001, "Heat transfer and fouling behavior of Siemens PWR steam generators-long-term operating experience," Experimental Thermal and Fluid Science 25 pp. 319-327.

Epstein, N., 1988, "General thermal fouling models," Fouling Science and Technology, Melo, L.F., *et. al.* (eds.), Kluwer Academic Publishers, Netherlands, pp. 15-30.

Forster, M., and Bohnet, M., 2000, "Modification of molecular interactions at the interface crystal/heat transfer surface to minimize heat exchanger fouling," Int. J. Therm. Sci. 39, pp.697-708.

Kern, D.Q. and Seaton, R.E., 1966, "Heat exchanger design for fouling surfaces," Chem. Eng. Prog. Vol. 62, No. 7, pp. 51-56.

Kim, W.T., Cho, Y.I., and Bai, C., 2001, "Effect of electronic anti-fouling treatment on fouling mitigation with circulating cooling-tower water," Int. Comm. Heat Mass Transfer, Vol. 28, No. 5, pp. 671-680.

Knudsen, J.G., 1986, "Functional correlation of surface temperature and flow velocity on fouling of cooling-tower water," Heat Transfer Eng., Vol. 7, pp. 63-71.

Li, W., and Webb,R.L., 2000, "Fouling in enhanced tubes using cooling tower water, Part II: combined particulate and precipitation fouling," Int. J. Heat and Mass Transfer 43, pp.3579-3588.

Reitzer, R.B., 1981, "Design of heat exchangers for effective heat transfer," Chem. Eng, No. 367, pp. 162-167.

Taborek, J., Aoki, T., Ritter, R.B., Palen, W., and Knudsen, J.G., 1972, "Predictive methods for fouling behavior," Chem. Eng. Prog., Vol. 68, No. 7, pp. 69-78.

Watkinson, A.P., Louis, L., and Brent, R., 1974, "Scaling of enhanced heat exchanger tubes," Can. J. Chem. Eng., Vol. 52, pp. 558-562.

Watkinson, A.P., 1980, "Process heat transfer: Some practical problems," Can. J. Chem. Eng., Vol. 58, pp. 553-559.

Webb.R.L., and Li,W., 2000, "Fouling in enhanced tubes using cooling tower water, Part I: long-term fouling data," Int. J. Heat and Mass Transfer 43, pp.3567-3578.